Journal Pre-proof

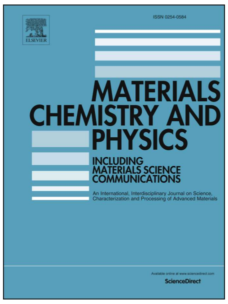

Synthesis of Magnesium Metallophosphate Bluish Pigment for Thermo-Reflective Coatings Using Cassava Polysaccharide Combustion

Nayara Balaba, Julia de O. Primo, Dienifer F.L. Horsth, Polona Umek, Carla Bittencourt, Fauze J. Anaissi

PII: S0254-0584(26)00829-1

DOI: https://doi.org/10.1016/j.matchemphys.2026.132836

Reference: MAC 132836

To appear in: *Materials Chemistry and Physics*

Received Date: 12 November 2025

Revised Date: 29 May 2026

Accepted Date: 21 June 2026

Please cite this article as: N. Balaba, J.d.O. Primo, D.F.L. Horsth, P. Umek, C. Bittencourt, F.J. Anaissi, Synthesis of Magnesium Metallophosphate Bluish Pigment for Thermo-Reflective Coatings Using Cassava Polysaccharide Combustion, *Materials Chemistry and Physics*, https://doi.org/10.1016/j.matchemphys.2026.132836.

This is a PDF of an article that has undergone enhancements after acceptance, such as the addition of a cover page and metadata, and formatting for readability. This version will undergo additional copyediting, typesetting and review before it is published in its final form. As such, this version is no longer the Accepted Manuscript, but it is not yet the definitive Version of Record; we are providing this early version to give early visibility of the article. Please note that Elsevier's sharing policy for the Published Journal Article applies to this version, see: https://www.elsevier.com/about/policies-and-standards/sharing#4-published-journal-article. Please also note that, during the production process, errors may be discovered which could affect the content, and all legal disclaimers that apply to the journal pertain.

© 2026 Published by Elsevier B.V.

Synthesis of Magnesium Metallophosphate Bluish Pigment for Thermo-Reflective Coatings Using Cassava Polysaccharide Combustion

Nayara Balaba[1,2*], Julia de O. Primo[1], Dienifer F. L. Horsth[1,2], Polona Umek[3], Carla Bittencourt[2], Fauze J. Anaissi[1*]

[1] Department of Chemistry, Universidade Estadual do Centro-Oeste, UNICENTRO, Alameda Elio Antonio Dalla Vecchia, 838, 85040-167, Guarapuava, PR, Brazil

[2] Chimie des Interactions Plasma-Surface (ChIPS), Research Institute for Materials Science and Engineering, University of Mons, 7000 Mons, Belgium

[3] Solid State Physics Department, Jožef Stefan Institute, 1000 Ljubljana, Slovenia

*E-mail: anaissi@unicentro.br and nayarabalaba20@gmail.com

Journal Pre-proof

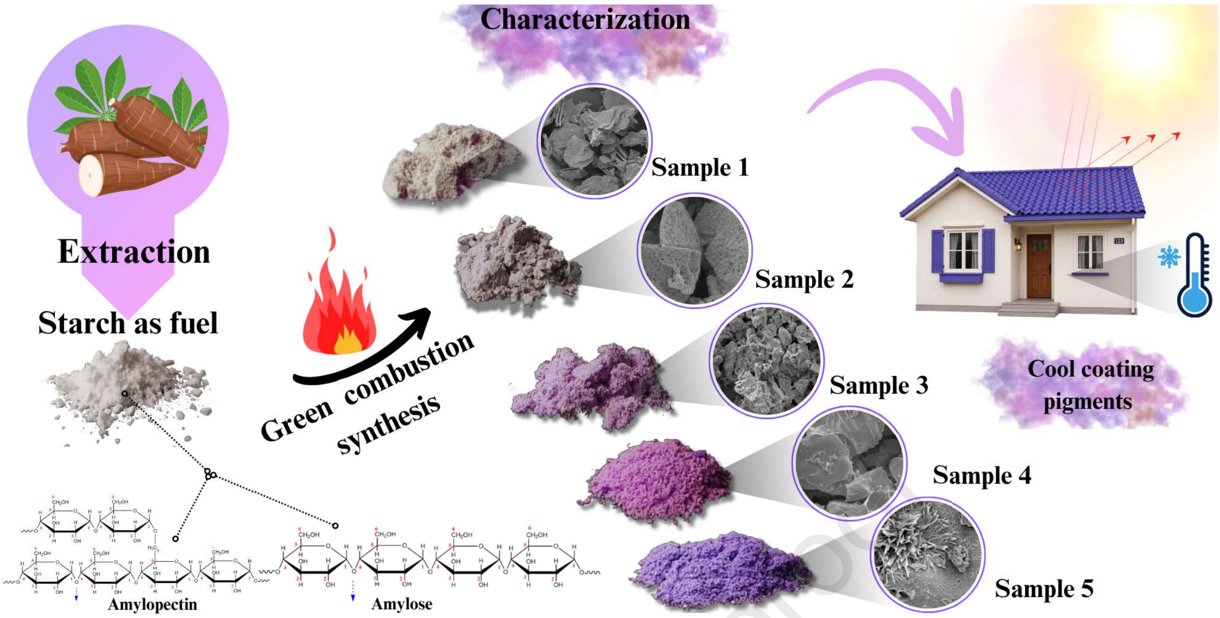

Journal Pre-proof

Abstract

This study explores cassava starch as a sustainable alternative for synthesizing metallophosphate pigments for reflective coatings. The study investigates the use of cobalt and alkaline ions to produce stable purple and pink pigments with enhanced reflective properties, addressing the environmental and economic dimensions of pigment synthesis. The synthetic methodology integrates starch as an organic fuel in a green combustion strategy, offering environmentally friendly and cost-effective pigment production. Characterization techniques have been used to assess the properties of the synthesized pigments, including X-ray diffraction, field emission scanning electron microscopy, X-ray photoelectron spectroscopy, and Fourier transform infrared spectroscopy. The $Co_xMg_{1-x}PO_4$ and $LiCo_xMg_{1-x}PO_4$ pigments showed discernible improvements in NIR reflectance among the synthesized samples, achieving solar reflectance values (R%) of 75% and 70%, respectively. These findings emphasize the importance of composition in determining pigments' reflective properties, which are essential for their use in practical applications requiring thermal insulation and color aesthetics.

Keywords: cassava starch; blue colors: cool pigments; NIR reflectance; colorimetry.

Journal Pre-proof

1. Introduction

The recent increase in atmospheric temperatures, attributed to rising CO2 emissions and the intensifying urban greenhouse effect, is a significant concern.[1] This phenomenon is associated with the decline in reforestation efforts in urban regions, exacerbating urban heat islands and leading to elevated temperatures compared to rural areas.[2] This situation has increased energy consumption for cooling, heat-related health problems, and mortality.[2] Therefore, the development of coating materials for passive cooling has become increasingly important. These materials reflect near-infrared (NIR) radiation in the solar spectrum, effectively reducing heat accumulation indoors and enhancing urban thermal comfort.[3,4] Inorganic pigments such as TiO_2 and ZnO are commonly used due to their inherent white color and reflectivity.[5] However, the plain white color may lack the vibrancy of colorful alternatives. Therefore, research in cool coatings focuses on novel synthesis methods of original colored pigments, such as yellow-colored $BiVO_4$,[6] and blue-colored YInMn,[4] to address this challenge.

Journal Pre-proof

Synthetic inorganic pigments have a long history and remain widely used due to their diverse properties and applications. Colors like purple, pink, and blue are highly valued for their association with royalty, distinctiveness, and sophistication.[7] The use of cobalt (Co) as a chromophore ion in the synthesis of purple-blue pigments has been highlighted in various studies.[3,7–9] When combined with lithium ions, pink-magenta tones can be achieved. The oxidation state, coordination number, and geometry of the cobalt ion play a fundamental role in determining the final color, ranging from violet to blue. The versatility of the Co^{2+} chromophore across different geometries, including tetrahedral, trigonal bipyramidal (TBP), square pyramidal, and octahedral, enables a range of colors and shades.[10] However, the extensive use of cobalt in electric vehicle battery production has led to its classification as a ‘critical raw material’ due to scarcity.[11] Therefore, efforts are focused on optimizing syntheses to reduce cobalt usage in purple-blue synthetic pigments.[9]

Transition metal phosphates (TMPs), including cobalt phosphates, show promise as matrices for material engineering and are being investigated for various applications such as sorbent anodes, rechargeable batteries, thermo-resistant materials, glasses, and pigments for reflective coatings.[9,12–15] TMPs can form solid solutions by accommodating different metal substitutions, leading to the synthesis of ceramic pigments based on different phosphates.[9] Phosphates form stable complexes with metal ions, particularly those of hard or intermediate ones. For example, metal ions like Mg^{2+} form complexes of a hard nature, while Co^{2+} exhibits an intermediate nature. Additionally, alkaline ions like Na^+ and Li^+ are known to form hard complexes.[16]

Common methods for synthesizing TMPs include the precipitation of inorganic metal salts with phosphorus precipitant,[15] sol-gel[17] or solvothermal methods,[18] solid-state maceration of salts[3] and phosphates under high-temperature high-pressure (HTHP) conditions[19]. The proposed synthesis approach involves using green combustion chemistry to synthesize metallophosphates and use them as inorganic pigments. The method includes synthesizing a green combustion solution using starch as the organic fuel. Starch decomposes upon heating, releasing volatile gases that sustain combustion.[20] Starch also acts as a reducing agent, aiding in the reduction of metal ions to metal nanoparticles.[21]

This study emphasizes pigment synthesis, focusing on minimal environmental impact, enhanced chemical reactivity, efficient combustion, reduced calcination temperature, and the use of plant polysaccharides as a fuel source.[5,22] Cassava starch (*Manihot esculenta*) was used as the polysaccharide source.[22] The research explores various combinations of alkaline, alkaline-earth, and transition-metal ions to synthesize phosphate-based pigments, aiming to develop vibrant, stable, and cost-effective pigments. By doping magnesium metal phosphates with cobalt and alkaline ions (Na^+ and Li^+), stable purple and pink pigments with reduced firing time and improved reflective properties were achieved.

2. Materials and Method

2.1 Reagents

The reagents used to synthesize the pigments were of analytical purity and had not undergone any prior treatment: cobalt(II) chloride ($CoCl_2{\cdot}6H_2O$, 98%, NEON); monobasic ammonium phosphate ($NH_4H_2PO_4$, 98%, SYNTH); magnesium carbonate ($MgCO_3$, 99%, SYNTH); anhydrous sodium carbonate (Na_2CO_3, 99%, SYNTH); lithium chloride (LiCl, 99%, VETEC). The starch was extracted from fresh cassava, and the stalks were harvested in the region of the city of Palmital, in the state of Paraná, Brazil.

2.2 Synthesis of phosphate pigments

The pigments were synthesized from colloidal emulsions of cobalt, magnesium, and phosphate salts, with doping levels varying between Na and Li ions. The pigments were synthesized by the wet route in two steps. The labeled sample, formulations, and the amounts of each reagent in moles are shown in the reactions in Table 1.

Journal Pre-proof

Table 1. Nomenclature table and main reaction proposed for each pigment synthesized

Sample	Chromophore molar ratio	Proposed main reactions
Sample 1	**$MgPO_4$**	$2MgCO_3 + 2NH_4H_2PO_4 \rightarrow Mg_2P_2O_7 + 2CO_{2(g)} + 2NH_{3(g)} + 2H_2O_{(v)}$
Sample 2	**$Co_{0.1}Mg_{0.9}PO_4$**	$3MgCO_3 + 2CoCl_2 + 2NH_4H_2PO_4 \rightarrow Co_2Mg_3PO_4 + 3CO_{2(g)} + 2Cl_{2(g)} + 2NH_{3(g)} + 3H_2O_{(v)}$
Sample 3	**$NaCo_{0.1}Mg_{0.9}PO_4$**	$0.5Na_2CO_3 + 0.9MgCO_3 + 0.1CoCl_2 + NH_4H_2PO_4 \rightarrow NaMg_{0.9}Co_{0.1}PO_4 + 1.4CO_{2(g)} + 0.1Cl_{2(g)} + NH_{3(g)} + 1.5H_2O_{(v)}$
Sample 4	**$LiCo_{0.1}Mg_{0.9}PO_4$**	$LiCl + 0.9MgCO_3 + 0.1CoCl_2 + NH_4H_2PO_4 \rightarrow LiMg_{0.9}Co_{0.1}PO_4 + 0.9CO_{2(g)} + NH_{3(g)} + 1.5H_2O_{(v)}$
Sample 5	**$LiNaCo_{0.1}Mg_{0.9}PO_4$**	$0.5Na_2CO_3 + LiCl + 4MgCO_3 + CoCl_2 + 4NH_4H_2PO_4 \rightarrow NaMg4(PO_4)_3 + LiCoPO_4 + 4CO_{2(g)} + 1.5Cl_{2(g)} + 4NH_{3(g)} + 5.5H_2O_{(v)}$

In the first synthesis step, the reagents were added to 50 mL of deionized water and homogenized under stirring for 1 hour. Subsequently, the mixture was heated to 150 ºC while stirring continuously for 90 minutes, forming a viscous liquid (Figure 1).

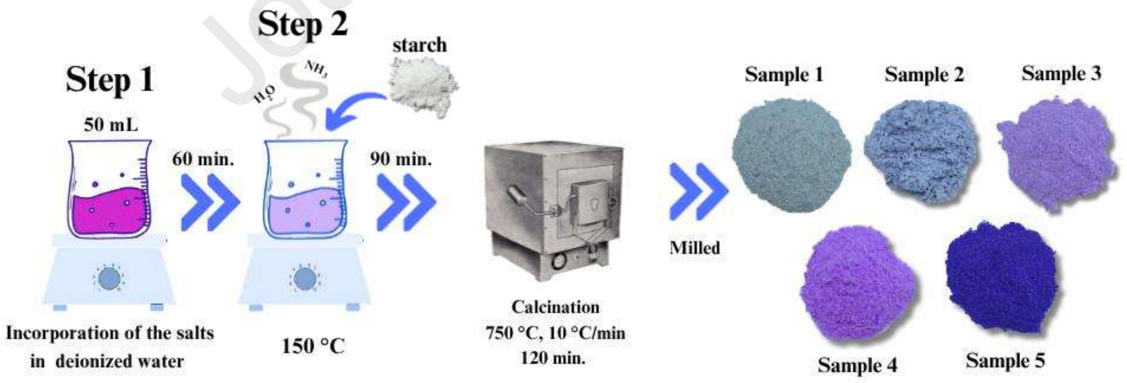

Figure 1. Scheme for synthesizing magnesium phosphate and cobalt pigments based on starch.

During this initial heating process, the volatile molecules of NH_3 and H_2O vapor are decomposed, helping maintain the solution's homogeneity with the precursors [3]. The colloidal suspensions of the pigments were calcined at 750 ºC for 2 hours with a heating ramp of 10 ºC/min. The resulting pigments are shown in Figure 1. The final step involved sample

Journal Pre-proof

cleansing, in which the samples were heated in a boiling aqueous solution for 15 minutes, then filtered; this process was repeated 5 times. Subsequently, the samples were dried at 70 °C for 24 hours. The pigments (Table 1) were macerated in an agate mortar and pestle set and then stored.

Characterization techniques

The samples were characterized by Powder X-ray diffraction (PXRD) (D2 Phaser, Almelo, Netherlands), equipped with a copper cathode (λ = 1.5418 Å), operated at 30 kV, current of 10 mA, with a working window between 10° and 80° (2θ) scanned with step of 0.026 θ/s. X-ray diffraction patterns were collected using a PANalytical Empyrean diffractometer operating in Bragg–Brentano θ/θ reflection geometry. Powdered samples were gently pressed onto the sample holder to ensure homogeneous distribution and mechanical stability during analysis. A spinning sample stage was employed during acquisition (1 s revolution time) to improve particle statistics and reduce preferential orientation effects. The morphology of the particulate samples was examined using a field-emission scanning electron microscope (FE-SEM, Verios G4, Thermo Fisher, Waltham, Massachusetts, USA). For the SEM analysis, the samples were dispersed in isopropyl alcohol, and a drop of dispersion was deposited on a polished Al sample holder. Before the SEM investigation, a ~5-nm-thick carbon layer was deposited on the specimens' surfaces. The oxidation state and chemical composition of pigments were determined by X-ray photoelectron spectroscopy (XPS) (Versaprobe PHI 5000, from Physical Electronics, Chanhassen, Minnesota, USA) equipped with a monochromatic Al Kα X-ray source. The spectra were analyzed by CASA-XPS software (Version 2.3.17PR1.1); the binding energies were calibrated using the C1s peak (284.6 eV) of carbon impurities as a reference. The Multipack version 9.8 software (ULVAC-PHI, 2017, Chigasaki, Japan) was used to evaluate the relative elemental composition. The chemical groups were identified, chemical bonds were determined, and the crystal structure was characterized using Fourier transform infrared spectroscopy (FTIR) (Perkin Elmer Frontier device, Waltham, Massachusetts, USA).

The samples were analyzed in ATR (Attenuated Total Reflection) mode. The sample was placed in direct contact with an ATR crystal, and the infrared light was transmitted through the crystal and into the sample for the formation of absorbance or transmittance spectra with a wider wavenumber. Samples were scanned from 650 to 4000 cm^{-1} at a spectral resolution of 4 cm^{-1}. To analyze the molecules, we also used Raman spectroscopy to study vibrational, rotational, and other low-frequency modes, which were recorded with a micro-Raman system (Senterra, Bruker Optik GmbH, Massachusetts, USA; λ = 532 nm; laser power = 10 mW). The

Journal Pre-proof

electronic spectra of the powdered pigment samples were measured over the range 400–900 nm (UV-Vis Ocean Optics spectrophotometer, model USB-2000, Dunedin, Florida, USA). The optical reflectance of the pigment powders and their corresponding coatings was measured using a UV-Vis-NIR spectrophotometer (PerkinElmer Lambda 950, Waltham, Massachusetts, USA). As a baseline standard, $BaSO_4$ was used to measure the optical properties of the samples between 300 and 2500 nm. The NIR solar reflectance (R*) of the pigments and coating in the wavelength range of 750–2500 nm was obtained by the following Equation (1), based on standard ASTM G173-03, which is the standard for reference solar spectral irradiance (amount of sunlight energy per wavelength) under clear atmospheric conditions. It was mathematically derived using the SMARTS (Simple Model for the Atmospheric Radiative Transfer of Sunshine) radiative transfer model[23–25]:

$$R *= \frac{\int_{750}^{2500} r(\lambda)i(\lambda)}{\int_{750}^{2500} i(\lambda)d(\lambda)} d(\lambda) \tag{1}$$

where r(λ) is the spectral reflectance obtained from the experimental, and i(λ) is the spectral irradiance obtained from the standard of ASTM G173-03 reference spectra ($W{\cdot}m^{-2}{\cdot}nm^{-1}$).

Laser scattering analysis was employed to determine the particle diameter of the samples. These measurements were carried out using Horiba's LA-960 laser-scattering particle-size distribution analyzer (Kyoto, Japan). Colorimetric analysis was carried out on the pigments in powder form and after application to plaster blocks, using a portable colorimeter (3nh, model NR60CP) with a D65 light source. The representative data from the colorimetric analyses (CIEL*a*b* Commission Internationale de l'Éclairage) are as follows: the L* parameter represents brightness and ranges from 0 to 100. The a* parameter represents the variation between red and green, where +a tends towards red and -a* tends towards green. The b* parameter represents the variation between blue and yellow, where +b* tends towards yellow and -b* tends towards blue. [26]. The total color deviation is expressed by the value of ΔE, which was created by the CIE to quantify the perceptual difference between two colors[27] and can be calculated using Equation (2):

$$\Delta E = \sqrt{(L_2{}^* - L_1{}^*)^2 + (a_2{}^* - a_1{}^*)^2 + (b_2{}^* - b_1{}^*)^2} \tag{2}$$

To interpret these ΔE values in the real world, we can assess them based on the intensity of the color difference. According to previous studies [26–28] colorimetric ΔE values can be classified as: color difference not perceptible (up to 0.2), very weak perception (0.2-0.5), weak (0.5-1.5), clear (1.5-3.0), very clear (3.0-6.0), strong (6.0-12.0), and very strong perception (above 12.0) [26,28].

2 Results and discussion

The importance of sample cleanliness evaluated by PXRD and mapping SEM/EDX

Horsth et al. [29] emphasized the formation of NaCl as a by-product when reagents containing sodium and chloride are utilized, necessitating a cleaning step for its removal. The presence of NaCl as a contaminant can significantly affect pigment properties, particularly stability. X-ray diffraction analysis of Sample 5 ($LiNaCo_{0.1}Mg_{0.9}PO_4$) before the cleansing process revealed characteristic peaks of the NaCl crystalline phase, and the disappearance of the main NaCl peaks was observed after the cleansing (Fig. 2a).

Journal Pre-proof

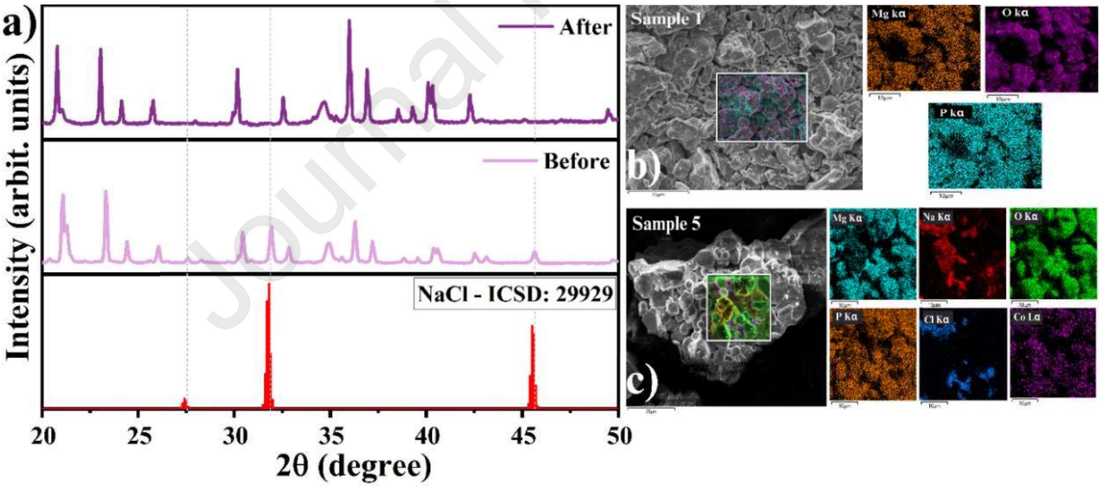

Figure 2. (a) Identification of the contaminating NaCl phase (ICSD database) in Sample 5 ($LiNaMg_{0.9}Co_{0.1}PO_4$), comparing before and after the cleaning step. Micrograph and chemical mapping of the undoped Sample 1 **(b)** shows the distribution of magnesium, phosphorus, and oxygen on the surface, represented by the colors orange, pink, and green, respectively. Sample 5(c) is doped with the chromophore cobalt and the alkali ions Na and Li.

Furthermore, elemental mapping via SEM/EDX of Sample 5 before cleansing indicated the presence of excess NaCl with uniform distribution (Fig. 2c). In contrast, the elemental distribution on the surface of Sample 1 (MgPO4) shows the absence of NaCl (Fig. 2 b), revealing only magnesium phosphate (Mg, O, and P) with a homogeneous distribution throughout the substrate.[30] Therefore, before the cleansing step, samples doped with lithium and cobalt exhibited excess chloride, resulting from precursor salts that formed NaCl.[8] Following this observation, all samples were cleaned using the process described in the experimental part.

Surface morphology study by scanning electron microscopy

Figure 3 shows the surface morphology of sample 1 as determined by scanning electron microscopy (SEM) analysis. In Fig. 3a, a structure resembling irregularly stacked platelets is evident. The magnified image (Fig. 3b) reveals numerous pores within the platelet structures, indicating that H_2O vapor and volatile substances such as NH3 played a significant role in generating porosity in this sample [31].

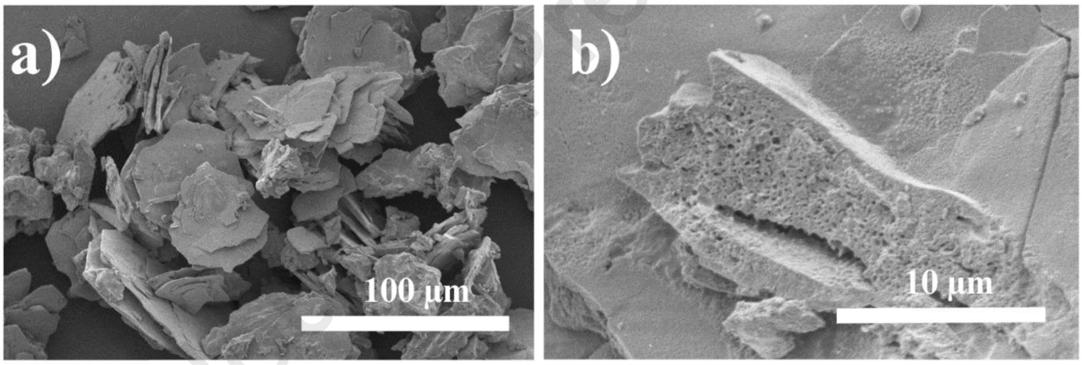

Figure 3. Micrograph of the undoped Sample 1 with cobalt or alkaline ions. The micrographs at 100µm (a) and 10 µm (b).

Upon cobalt ion addition, sample 2 ($Co_{0.1}Mg_{0.9}PO_4$) shows a similar platelet-like morphology characterized by disordered arrangement and varying thicknesses (Fig. 4a). The magnified view in Fig. 4b reveals irregular surfaces and small pores within each platelet; this morphology was attributed to uncontrolled and spontaneous combustion.[32] Additionally, Figs. 4c and 4d show the morphology of sample 3 ($NaCo_{0.1}Mg_{0.9}PO_4$), displaying a disordered morphology of large, irregularly shaped particles with varying sizes, as well as agglomerates of small pseudo-spheres. This morphology is likely to result from the release of a substantial amount of gas during combustion synthesis [33,34].

The morphology of sample 4 ($LiCo_{0.1}Mg_{0.9}PO_4$) (Fig. 4e and 4f) is characterized by large particles with a rough surface, cracks, and small particles distributed on the surface of larger particles (marked by the red circle in the image). Upon analyzing the micrograph of Sample 5 (Fig. 4g and 4h), the images reveal the formation of stacked particles in a layer-by-layer configuration, characteristic of olivine-type $LiMgPO_4$ structures [35] along with aggregates of small pseudo-spheres as observed in the surface of $NaMg_3(PO_4)_3$ as described by Zhou.[34] The formation of a flower-like morphology was observed in the LiCoPO4 olivine phase; this morphology was reported to depend on the organic additive and its concentration used in the synthesis [36].

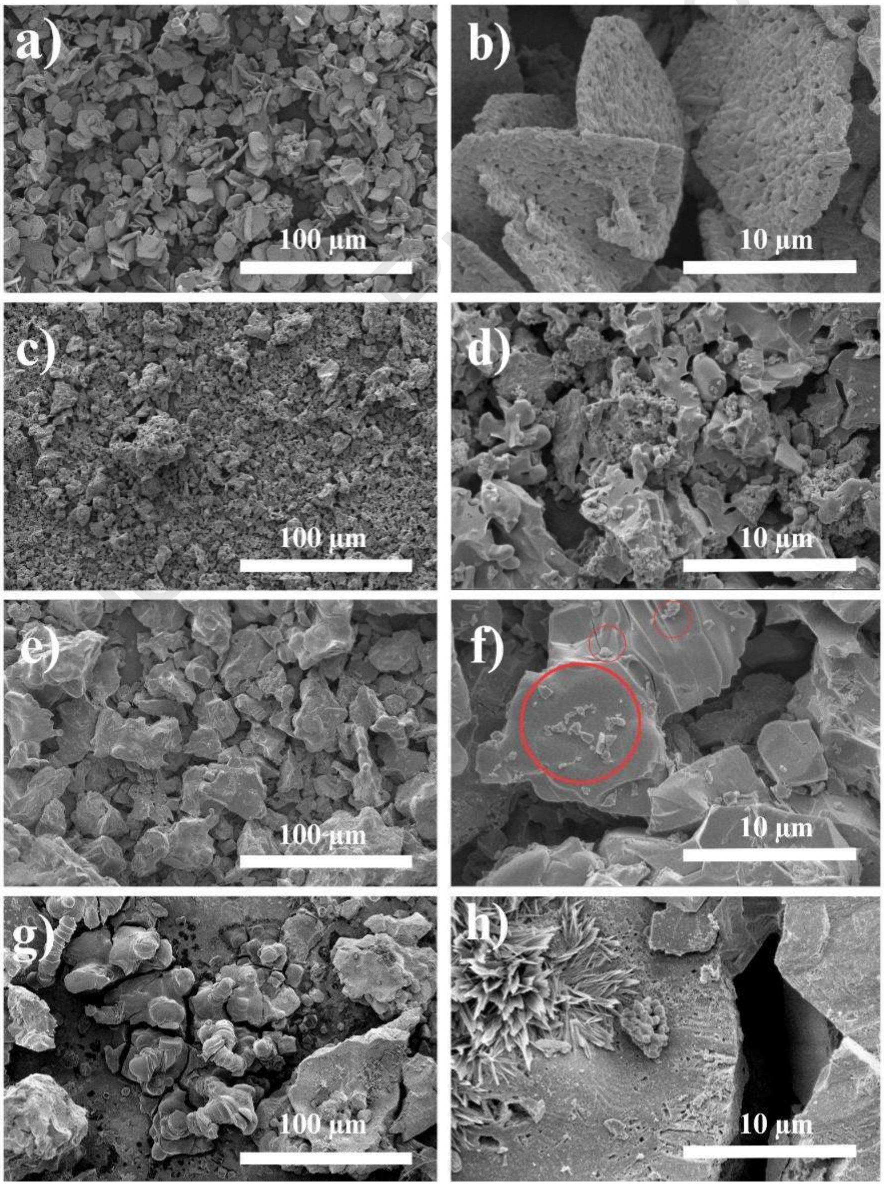

Figure 4. Micrographs of the pigments (a-b) Sample 2; (c-d) Sample 3; (e-f) Sample 4 and (g-h) Sample 5.

Structural phase by PXRD

The crystalline structure of the pigments was identified using X-ray diffractometry following the cleansing stage. The diffractograms were identified and processed using Match! software and the ICSD database (COD). Sample 1 (Fig. 5a) shows the beta magnesium pyrophosphate crystallographic phase β-$Mg_2P_2O_7$ (COD:15326), which crystallized in the monoclinic space group C_2/m-$C_3$2h. Simple diphosphates (or pyrophosphates) typically have two structural variants that depend on the formation temperature: the α structure at low temperatures and the β structure at high temperatures, precisely above 500 ºC.[37]

The analysis of Sample 2 (Fig. 5b) revealed the same crystallographic structure as Sample 1, magnesium cobalt diphosphate β-$Mg_2P_2O_7$ (COD:15326). This phase belongs to the monoclinic system and crystallizes in the space group P21/C (14).[38]. This means the cobalt in the diphosphate structure resulted from the low concentration. This is because cobalt radio is similar to magnesium and can be incorporated into the magnesium phosphate host structure without disrupting it.[38]

The diffractogram for Sample 3 (Fig. 5c) matched the monoclinic phase pattern of sodium magnesium orthophosphate $NaMg_4(PO_4)_3$ (COD:35496). This compound crystallizes in the orthorhombic structure with a space group Pnma (62), featuring a three-dimensional network composed of [PO_4] tetrahedra and [MgO_5] polyhedra interconnected by P-O-Mg bridges.[39] Additionally, specific peaks correspond to the crystallographic phases $Co_2P_2O_7$ and $Mg_2P_2O_7$ at 29.6°, 35.5°, 36.9°, 43.1°, and 55.9°, respectively.

The XRD profile for Sample 4 (Fig. 5d) shows a mixture of two phases, $LiMg_3(PO_4)P_2O_7$ (COD:428811) with an orthorhombic cell structure and Pnma (62) space group (Fig. 4Sd). This structure incorporates mixed anion phosphates, where orthophosphate and pyrophosphate anions coexist as independent units.[40] The main structural characteristics of $LiMg_3(PO_4)P_2O_7$ include infinite [Mg3O10] parallel layers along the bc plane, interconnected along an axis, and alternating PO4 and P2O7 chemical groups that form large tunnels along the two crystallographic directions.[40] The second phase identified was $LiCoPO_4$ (COD:14847), also known as Olivine, which crystallizes in the orthorhombic structure with space group Pnma.

The crystal structure of LiCoPO4 consists of octahedral cobalt atoms and tetrahedral phosphorus atoms linked to oxygen atoms shared at the corners or edges, with lithium ions incorporated into octahedral vacancies in the crystal lattice.[41] Fig. 5 (e) shows the XRD pattern for the Sample 5 pigment, revealing three main phases: lithium magnesium phosphate

Journal Pre-proof

($LiMgPO_4$ COD:11770), sodium magnesium orthophosphate $NaMg_4(PO_4)_3$ (COD:35496), and lithium cobalt phosphate ($LiCoPO_4$ COD:14847). $LiMgPO_4$ crystallizes in orthorhombic systems, where the tetrahedral PO_4, octahedral LiO_6, and MgO_6 groups constitute the structure, forming the 3D crystal lattice [42].

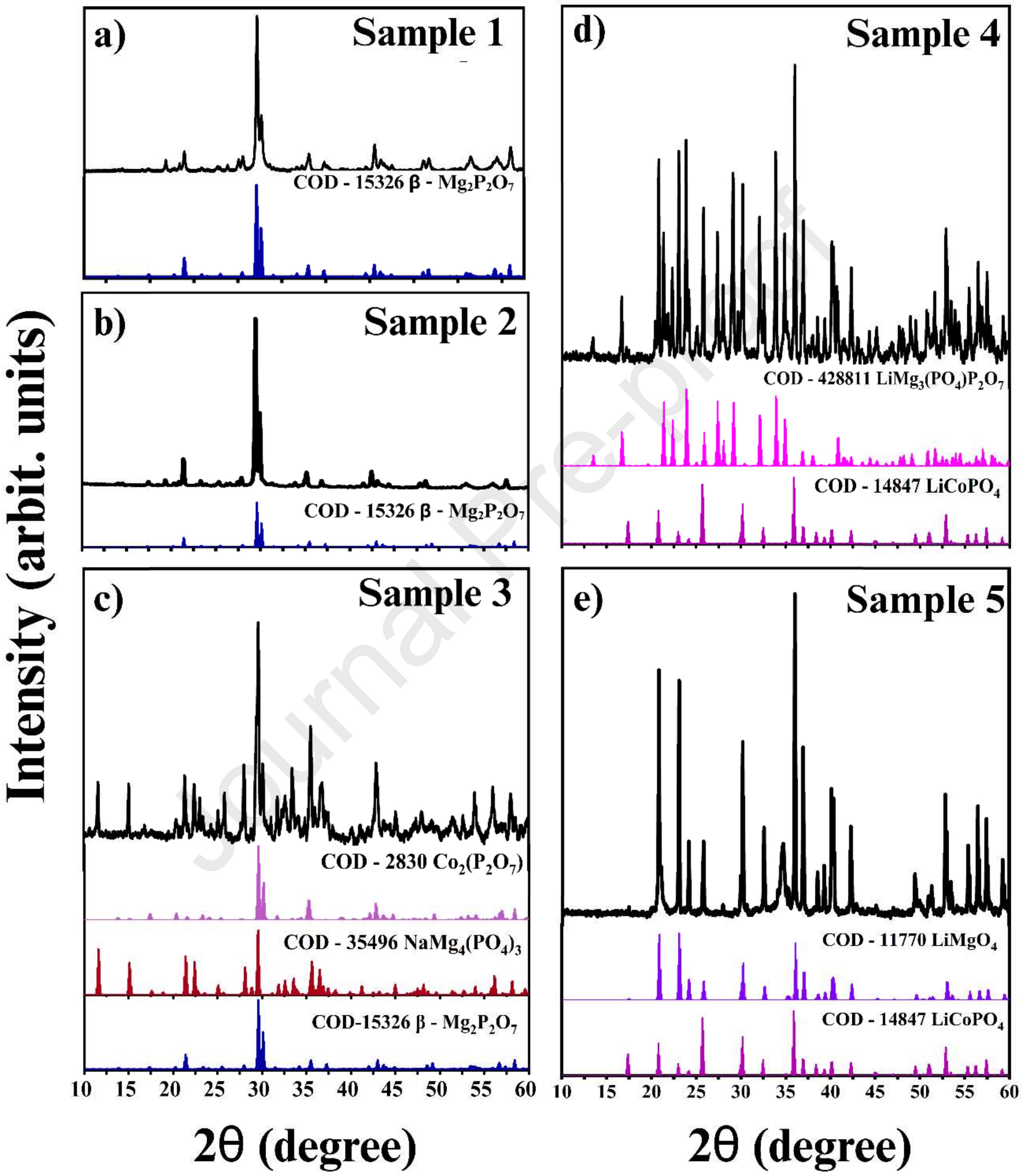

Journal Pre-proof

Figure 5 - X-ray diffractograms for pigments a)Sample 1; b) Sample 2 c) Sample 3; d) Sample 4 and e) Sample 5.

Meanwhile, the three-dimensional network structure of $LiCoPO_4$ comprises octahedra [CoO_6], tetrahedra [PO_4], and Li^+ ions in octahedral voids.[43] These compounds belong to a large family of orthophosphates with the general formula $ABPO_4$ and their structure depends on the relative size of the ions. For instance, in the case of $LiMgPO_4$, where the sizes of the monovalent A (Li^+) and bivalent B (Mg^{2+}/Co^{2+}) ions are relatively small, the final compound adopts the structure of olivine.[42] Figure 4S shows the comparison of diffractograms after cleansing Sample 5, in which the secondary phase of the NaCl formed was reduced.

Samples 3, 4, and 5 showed more than one phase by PXRD, it is not uncommon for synthetic inorganic pigments to have more than one crystalline phase, especially when it comes to metal oxides and other complex compounds. During pigments synthesis, different crystalline phases can form due to variations in the synthesis parameters, such as the calcination temperature. In this work we propose a synthesis using starch as the green fuel for combustion and formation of the materials, aiming for a lower burning temperature and lower costs, adding alkali metals such as Li and Na to vary and intensify the colors of the materials without increasing the amount of cobalt ions (a relatively more expensive metal). As phosphates are compounds that can include different metals, the exact composition can influence the formation of various crystalline phases. Variations in the proportion of constituent elements can lead to the coexistence of different phases. There are studies of phosphate pigments that have more than one phase, such as cobalt/iron[44], strontium/zinc[45], and strontium/calcium/aluminium[46] phosphates.

In order to verify the thermal stability of the phases obtained, a test was carried out. The powdered pigments were heated to a temperature of 1000 ºC with a ramp of 10 ºC/min for 2 hours. After this experiment, the XRD analysis was redone and we observed that the existing phases remained the same. However, the intensities of the diffractogram peaks slight changed. The increase in the intensity of the X-ray diffraction peaks after heating the samples is directly related to an improvement in the crystalline order of the material. This may have occurred due to the growth of grains and reduction of structural defects during the sintering of the samples.[47] In the supplementary materials, Figure 1S shows the diffractogram data after calcining the pigments in powder.

Chemical characterization by XPS

XPS was used to study the chemical composition of the samples after cleansing (Table 2). The higher concentration of Na than Li can be related to a better incorporation of Li in the bulk of the material and a migration of Na to the surface. As XPS is a highly surface-sensitive technique, it detects electrons from only the first few nanometers of the sample. If lithium is present at a very low concentration beneath the surface layer, the technique may not detect it.[48]

Journal Pre-proof

The presence of carbon can be linked to byproducts of carbonate salts used in the synthesis ($MgCO_3$ and Na_2CO_3). Also, it can be attributed to residual carbonaceous species originating from cassava starch used during synthesis, in addition to adventitious surface carbon commonly observed in air-exposed samples[49]. It is important to emphasize that no secondary crystalline carbon-containing phases were identified in the XRD patterns, indicating that the residual carbon is predominantly amorphous/surface-related and does not affect the structural formation of the synthesized phosphate materials.

Table 2. Composition of the samples after the cleansing step according to XPS.

Sample	Elements (atm%)							
	C	O	Mg	P	Co	Li	Na	Cl
Sample 1	14.7	61.1	9.0	15.2	-	-	-	-
Sample 2	13.7	60.1	9.9	15.3	1.0	-	-	-
Sample 3	18.3	54.3	12.9	10.4	1.1	-	3.0	-
Sample 4	13.3	57.5	6.0	13.7	1.7	6.7	1.1	-
Sample 5	14.0	52.8	5.4	10.8	3.5	2.9	10.6	-

The XPS spectra in the Mg 1s, O 1s, and P 2p binding energy range are shown in Fig. 6. The spectra were calibrated based on the C 1s reference peak at 284.6 eV and reproduced using Gaussian-Lorentzian function (GL30%) components. The Mg 1s XPS spectra were reproduced using a single component, centered at 1303.5 eV attributed to Mg in Mg-O bonds in the phosphate structure, corresponding to the Mg^{2+} ion.[50]. The P 2p spectra were reproduced using two doublets, corresponding to the 2p3/2 and 2p1/2 components. The component P 2p3/2 centered at 134.0 eV is consistent with the presence of pentavalent tetracoordinate phosphorus found in phosphates and/or polyphosphates in O=P-O bonds.[51] These results support the formation of metallophosphates, suggesting the presence of the structure $Mg_2P_2O_7$,[52] which aligns with the phase identified through XRD.[53] The doublet with the 2p3/2 component centered at 132.8 eV is attributed to the presence of phosphine oxide species in O-P-C bonds.[54].

The O 1s XPS spectra of samples 1, 2, 3, and 4 were reproduced with three components (Gaussian-Lorentzians), component 1, centered at 531.5 eV, corresponding to the Co-O bond [53], consistent with the $Co_2P_2O_7$ structure identified by XRD.

Journal Pre-proof

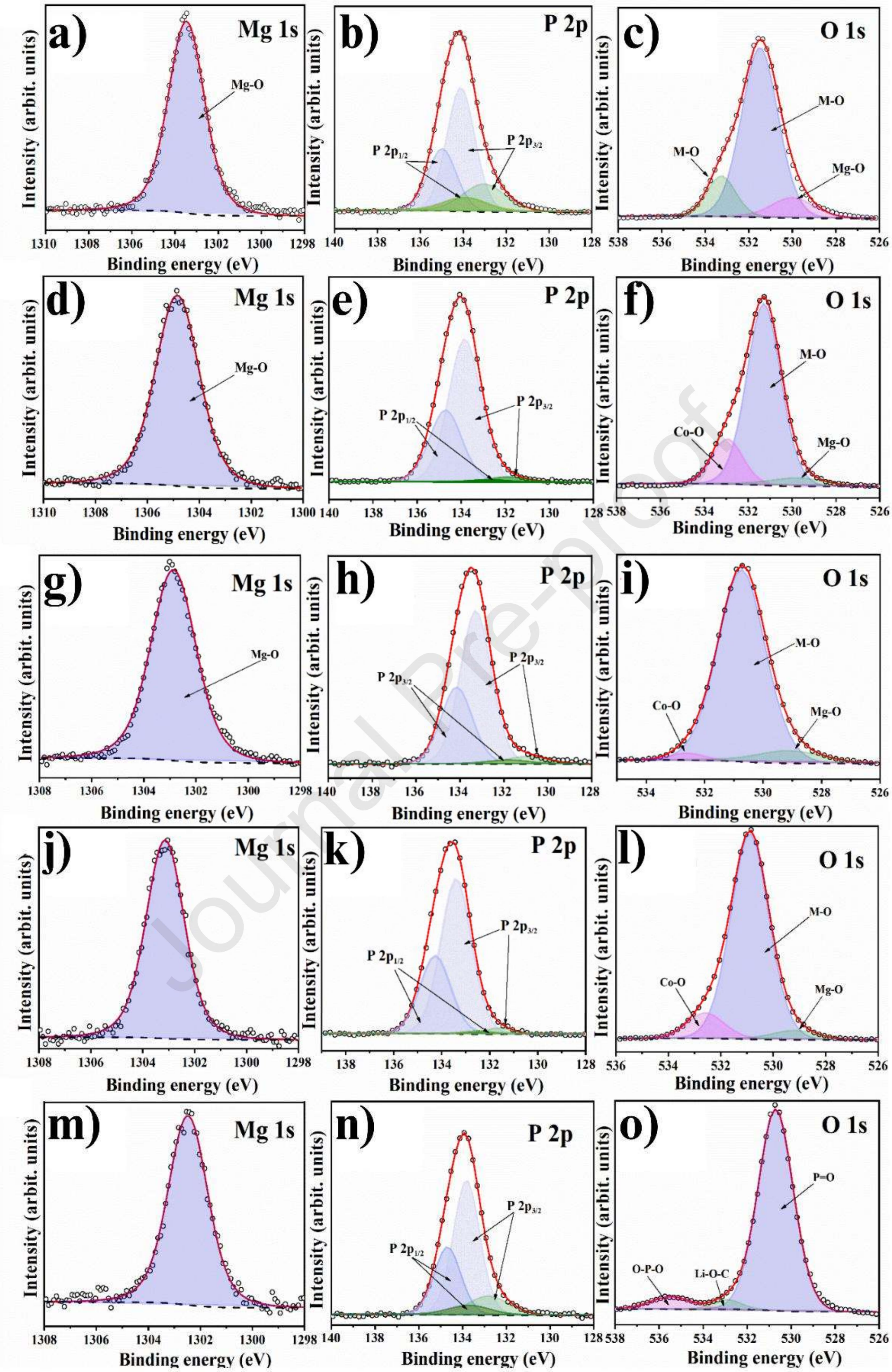

Journal Pre-proof

Figure 6. XPS of the Sample 1 (a, b, c); Sample 2 (d, e, f)); Sample 3 (g, h, i); Sample 4 (j, k, l) and Sample 5 (m, n, o) for the center level spectra of the elements Mg 1s, P 2p and O 1s.

Component 2, centered at 529.9 eV, attributed to the Mg-O bond,[52] and component 3, centered at 533.3, corresponding to oxygen bound to metals (M-O) such as Co, P, or Mg [55]. The O 1s spectrum of Sample 5 (Fig 6 o) reproduced with three components centered at 530.7, 532.9, and 535.4 eV associated with lattice oxygen (O^{2-}). This refers to oxygen doubly bound to phosphorus (P=O), lithium carbonate ($LiCO_3$) formed from carbonate salts, and oxygen singly bound to two phosphorus atoms (O-P-O), respectively.[56,57]

Figure 7 shows the Co $2p_{3/2}$, Na 1s, and Li 1s photoelectron spectra. The Co $2p_{3/2}$ spectrum for Sample 2 (Figure 7a) was reproduced using six components: the components centered at 775.5 and 780.2 eV are associated with the Co LMM Auger peaks [58]. The components centered at 782.7 eV and 784.5 eV are characteristic of Co^{2+} ions in CoO (tetrahedral coordination) and in Co(OH)2, respectively [59,60].

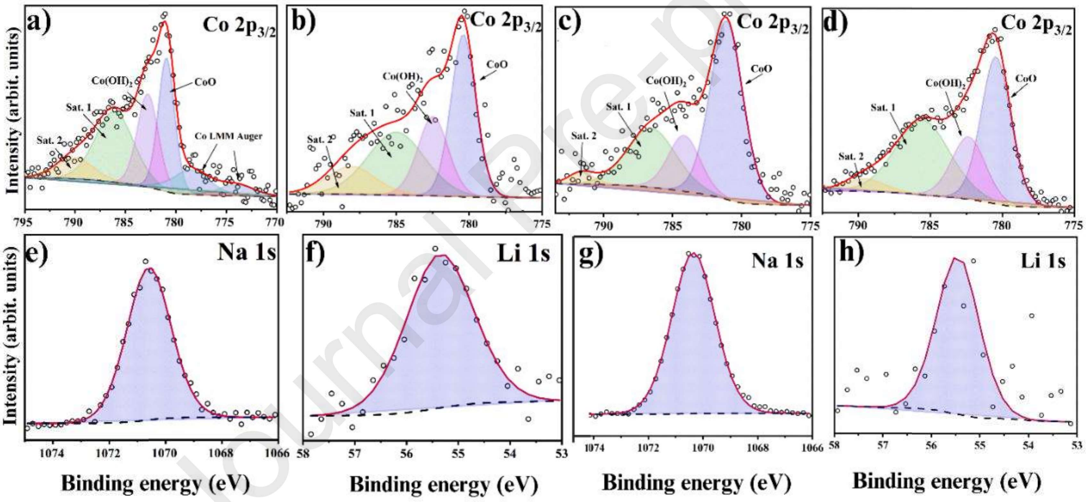

Figure 7. XPS of the pigments Sample 2 (a), Sample 3 (b), Sample 4 (c), and Sample 5 (d) for the center level spectra element Co 2p. XPS and Sample 3 (e); Sample 4 (f), Sample 5 (g and h), for the center level spectra of the elements Na 1s and Li 1s.

Journal Pre-proof

The $Co(OH)_2$ component indicates that the surface of the pigment particles is hydrated. The components at 787.9 eV and 791.9 eV are the respective satellites of the CoO and Co(OH)2 components, further demonstrating the presence of cobalt oxides/hydroxides.[59,61] The Auger peaks were not observed in the Co 2p spectrum of the other samples. The Li 1s peak centered at 55.4 eV can be assigned to surface carbonate species (Li_2CO_3),[56] verifying the assignment observed in the O 1s component (Fig. 5S d). The Na 1s spectra centered at 1070.4 confirm the presence of Na atoms occupying the lattice positions along the b-axis of sodium magnesium orthophosphate $NaMg_4(PO_4)_3$.[62] These values are those reported in the literature, confirming the presence of Na_2HPO_4-type structures [62].

Vibrational spectroscopy by FTIR and Raman

Figure 8a shows the FTIR spectra; the spectra of samples (2, 3, 4, and 5) exhibited a broad band centered at 3373 cm^{-1}, associated with the bond stretching of free water molecules (νOH), and at 1640 cm^{-1} corresponding to the bending vibration spectral region of the water molecules (δHOH). The broadening of the half-width of the signal for Sample 2 can be attributed to the strong interaction between water molecules and metal ions, indicating a gradual transformation of water from a free state to being confined/bound to the reaction products, affecting both for ν OH and δ HOH [63].

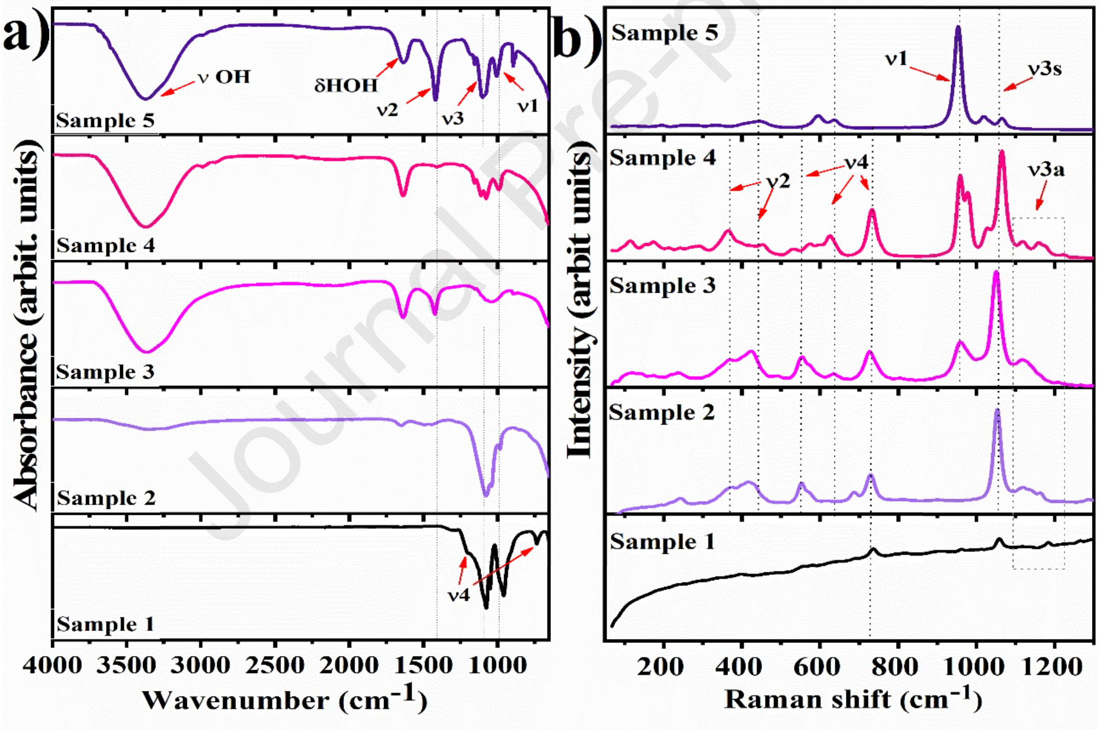

Figure 8. FTIR (a) and Raman (b) spectra of the metallophosphates pigments.

To characterize the metallophosphates, the features in the spectral range of 1200-650 cm^{-1}, where the primary vibrations of the phosphate groups are located.[63] The band centered at 1400 cm^{-1} corresponds to the asymmetric stretching vibrations of oxygen atoms doubly bonded to phosphorus, ν2(P=O); in tetrahedral structures, the pigments containing Na+ exhibit the highest relative intensity. Given the large nature of Na ions, they likely induce a polarization effect of the modifying cation (Na) on the P=O bond, resulting in a modification of the charge

Journal Pre-proof

density at the anionic site.[64,65] A band identified between 1100-1083 cm^{-1} corresponds to the asymmetric stretching of the P-O-P bonds in the pyrophosphate groups, ν_3(PO_3^{2-}). This interaction also polarizes the cation towards the P-O-H bond, although the P=O bond is more electron-rich than the O-H bond.[66] The band at 980 cm-1 in the middle represents the symmetric stretching mode of the phosphorus-oxygen bond, ν_1(P-O).[67]

Two low-intensity bands observed in the Sample 1 spectrum were not present in the spectra of the other samples. These bands, located at 735 cm^{-1} and 1226 cm^{-1}, are assigned to the asymmetric stretching vibration of the P-O-P group (ν_4 P-O-P), which is characteristic of the magnesium pyrophosphate phase $Mg_2P_2O_7$,[67,68] consistent with XRD data. The defects in the crystalline structure are attributed to the substitution of Mg^{2+} by Li^+, Na^+, or Co^{2+} ions [69].

The Raman spectra of the pigments are shown in Figure 8b. The Raman spectrum of Sample 1 exhibits three bands characteristic of the Mg_2PO_4 structure, aligning with the XPS and XRD analysis. These characteristic features of the β-$Mg_2P_2O_7$ structure are a peak middle at 1060 cm^{-1} attributed to the terminal symmetric P-O stretching mode (ν_{3s}P-O), a peak centered at 730 cm^{-1} associated with the symmetrical P-O stretching mode of the P-O-P bond (ν_4 P-O-P), and a low-intensity peak above 1100 cm^{-1} identified as the asymmetric P-O stretching modes (ν_{3a} P-O).[70] The 1060 and 730 cm^{-1} peaks are in the Sample 2, Sample 3, and Sample 4 spectra. However, only the Raman peak at 1060 cm^{-1} is observed in the Sample 5 spectra. Furthermore, the peak centered at 954 cm^{-1} originated from the symmetrical stretching vibration of the phosphate groups (non-degenerate ν_1P-O). This particular peak was detected exclusively in cobalt- and alkali-ion-containing materials, not in Sample 1, indicating that ionic substitution influences the material structure.[71] Other peaks were assigned as follows: at 363 and 432 cm^{-1} corresponding to the double degenerate single bond bending mode ν_2(O-P-O); and at 550, 593, and 630 cm^{-1} associated with the triple degenerate single bond bending mode, ν_4(O-P-O), with variation in relative intensity and widths of the peaks for all samples, except pristine Sample 1 [71].

Electronic spectrum (UV-VIS)

Figure 9a illustrates the UV-Vis absorbance spectrum of Sample 2, displaying multiple bands around 500 nm (463, 523, and 584 nm). This triplet is in agreement with the presence of the Co^{2+} ions in the octahedral and trigonal bipyramidal coordination, which represent the crystallographic sites for the cobalt ion in the structures.[38] The bands middle at 584 and 523 nm (corresponding to $^4T_1(F) \rightarrow {}^4A_2(F)$, $^4T_1(F) \rightarrow {}^4T_1(P)$ transitions, respectively) are attributed

Journal Pre-proof

to the spin-allowed transitions of Co^{2+} ions in an octahedral ligand field. In comparison, the band at 463 nm corresponds to the $^4A_2 \rightarrow ^4E(P)$ transition indicative of the transition of Co^{2+} in high-spin trigonal bipyramidal sites.[38] In contrast, the absorption spectrum of sample 3 (Fig.9 b) exhibits a doublet between 500 and 600 nm. The $^4T_1g \rightarrow ^4T_1g(P)$ transition implies mixing the prohibited spin transitions for 2G and 2H derived doublet states, along with the weak $^4A_2 \rightarrow ^4E(P)$ transition, often appearing only as a shoulder [72].

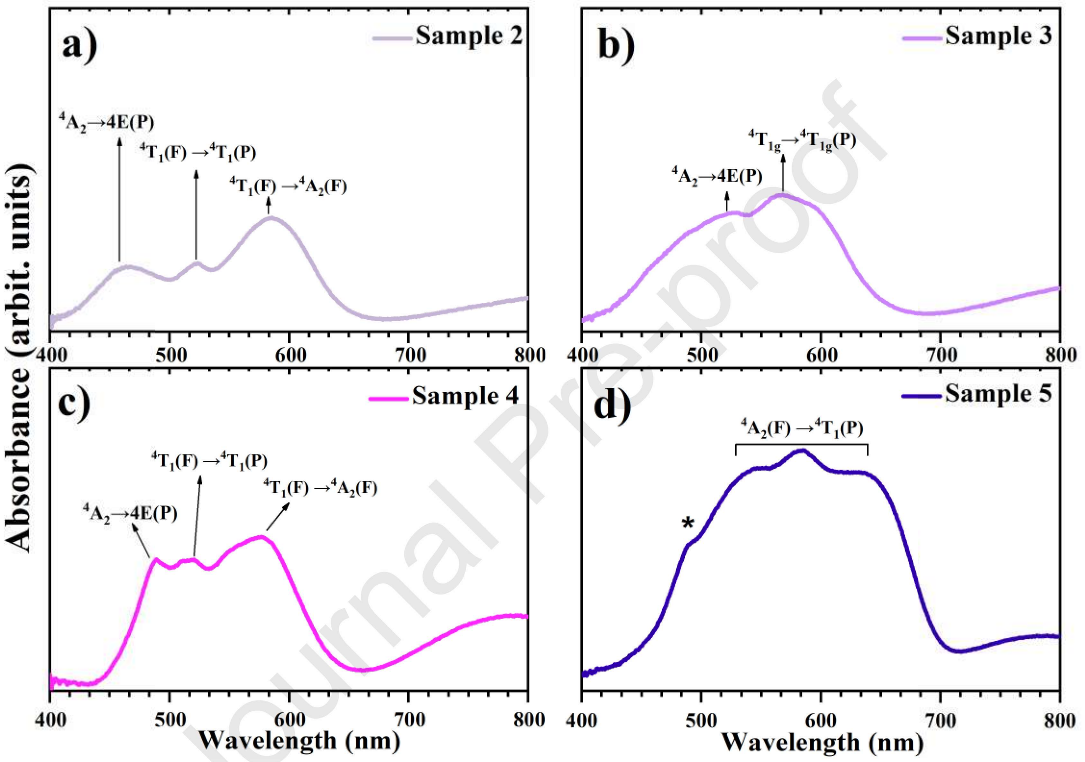

Journal Pre-proof

Figure 9. UV-vis absorbance spectra of Sample 2 (a), Sample 3 (b), Sample 3 (c), and Sample 3 (d) for pigments containing the chromophoric ion Co^{2+}, thus being able to interpret the transition bands d-d.

For Sample 4 (Fig. 9 c), the spectrum is similar to that of Sample 2 and Sample 5 (Fig. 9 a, d), showing identical d-d triplet electronic transitions as cobalt, albeit with broader and more intense bands than Sample 2. The splitting of the triplet in the high-energy absorption region was attributed to spin-orbital coupling (L-S Russell-Saunders) and Jahn-Teller distortion, leading to the broadened band.[73] In the absorbance spectrum of Sample 5 (Fig. 9 d), the bands became more pronounced, with the triplet of bands observed at 538, 580, and 635 nm associated with the d-d transition of the Co^{2+} ion $^4A_2(F) \rightarrow ^4T_1(P)$, a spin-allowed transition in tetrahedral geometries with Jahn-Teller distortion resulting in the bluish-purple hue.[26] The low-intensity bands around 487 nm (denoted by the symbol *) are linked to the spin-forbidden transition, attributed to transitions between octahedral and tetrahedral sites[74].

Even though all the pigments have the same chromophore ion (Co^{2+}), the different chemical environments modify the electronic distribution around the atoms or molecules, altering the energies of the possible electronic transitions. These changes in transition energies result in different absorption bands in the UV-Visible spectrum. Each change in the chemical environment can lead to subtle or significant changes in the optical properties of the substance[75].

NIR reflectance

Beyond their aesthetic properties, inorganic pigments are currently being investigated for their potential to mitigate the urban heat island effect. Figure 10 shows the NIR reflectance spectra of the pigments. Fig. 10a corresponds to the NIR reflectance spectrum adjusted according to the measurement standard JG/T235-2014, where the spectral reflectance is multiplied by the normalized solar hemispherical irradiance i (λ). Among the five synthesized samples, Sample 2, Sample 3, and Sample 4 exhibit a reflectance profile exceeding 60% characteristic of "cool" reflective inorganic pigments, indicating their capacity to function as cool pigments with enhanced thermal insulation properties for practical applications [74].

Journal Pre-proof

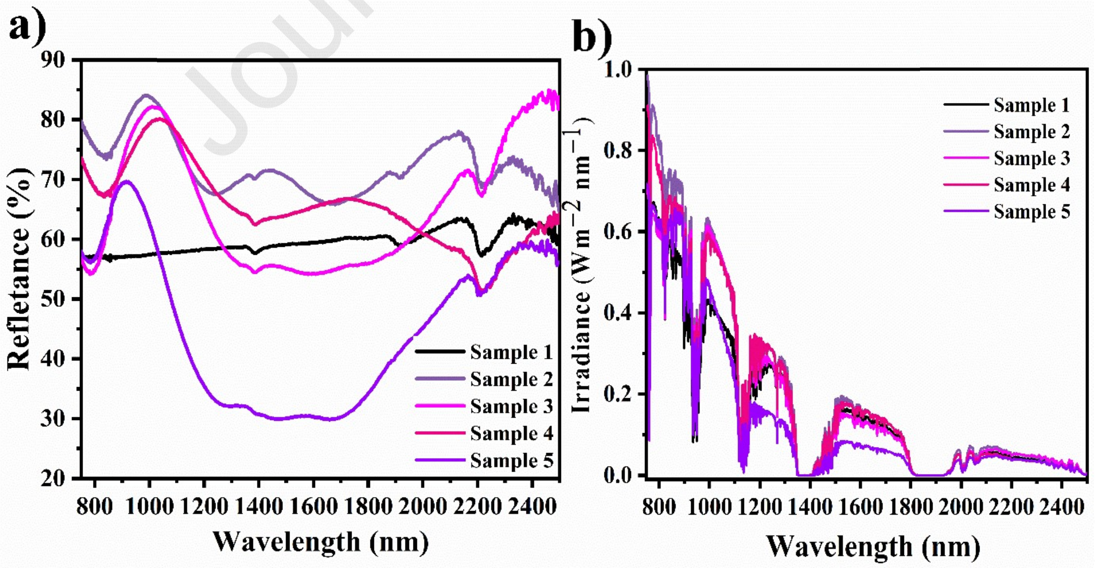

Figure 10. (a) Diffuse reflectance spectra of the powdered pigments synthesized, and (b) NIR solar reflectance spectra of the powdered pigments adjusted to the standard solar spectrum.

Notably, Sample 5 (Fig. 10a) demonstrated a substantial decrease in solar reflectance compared to the other samples, attributed to significant absorption in the 1200-1600 nm range due to d-d transitions for tetrahedral Co^{2+} ions [3], leading to pronounced absorption in the NIR region and the UV-Vis data for this pigment. The NIR solar reflectance curves of the pigment powder samples were calculated using the ASTM G173-03 standard (Figure 10 b). The $Co_xMg_{1-x}PO_4$ and (Li)$Co_xMg_{1-x}PO_4$ pigments slightly enhanced NIR reflectance compared to the other samples, with solar reflectance (R%) equal to 75% and 70%, respectively (Table 3).

According to the Kubelka-Munk theory, the reflectance of a material is inversely proportional to its particle size [1,74]. According to the theory, the average particle size (d) is inversely related to the scattering coefficient (S). Consequently, when the average particle size is smaller ($d < 1$ μm), the material's scattering efficiency increases, leading to a rise in reflectance [15]. In the current study, materials displaying superior NIR reflectance characteristics have an average particle size of 82 nm (Sample 2), 96 nm (Sample 3 nanospheres), and 250 nm (Sample 4). The morphology of the materials is another factor contributing to the enhanced reflectance. Deepa et al. reported that pigments with small particle sizes and a uniform, rough, plate-like morphology scattered incident radiation rapidly, thereby confirming an increase in solar NIR reflectance.[1] This morphology is similar to Sample 2, where the plate-like morphology was observed by SEM, validating the superior NIR reflectance result.

Pigments containing cobalt, alkali ions, rare earths, and phosphate - spinel-based that are potential candidates for cool pigments are presented in Table 3. The NIR reflectance values obtained in this work are comparable to those reported for previously published reflective pigments. Among the synthesized samples, Sample 2 ($Co_xMg_{1-x}PO_4$) exhibited the highest reflectance (75%), surpassing values reported for Elakkiya et all (2022)[76] with yellow pigment $FeP_{0.8}V_{0.2}O_4$ (72% of reflectance), $Zn_{0.9}Co_{0.1}Al_2O_4$ prepared by combustion synthesis (63%) [77] and $LiZn_{0.9}Co_{0.1}PO_4$ synthesized by coprecipitation (68%) [15], while remaining close to the $LiMg_{1-x}Co_xPO_4$ system prepared by solid-state maceration (74%). In contrast, Samples 1 and 5 showed lower reflectance values (58% and 51%, respectively), which may be associated with differences in composition and scattering behavior. These variations demonstrate that both the cationic composition and synthesis route strongly influence the optical properties of reflective pigments. Furthermore, the colloidal suspension method using cassava starch employed in this work proved effective for producing phosphate-based pigments with competitive reflectance performance for potential cool-coating applications.

Journal Pre-proof

Table 3. Phosphate-based pigments, their respective synthesis methods, and NIR reflectivity.

Samples	Method	Reflectance (%)	Reference
$LiMg_{1-x}Co_xPO_4$	Solid-state maceration	74	[78]
$NaZn1-xCoxPO_4$		49	
$LiZn_{0.9}Co_{0.1}PO_4$	Co-precipitation	68	[79]
YPO_4		68	[15]
$YP_{0.6}V_{0.4}O_4$		64	
$FeP_{0.8}V_{0.2}O_4$		72	[76]
$Zn_{0.9}Co_{0.1}Al_2O_4$	Combustion	63	[77]
$Mg_{0.5}Co_{0.1}Mn_{0.4}Al_2O_4$	Spray pyrolysis	32	[80]
$Mg_{1-x}PO_4$ (Sample 1)	Colloidal suspension with starch	58	This work
$Co_xMg_{1-x}PO_4$ (Sample 2)		75	
$NaCo_xMg_{1-x}PO_4$ (Sample 3)		66	
$LiCo_xMg_{1-x}PO_4$ (Sample 4)		70	
$LiNaCo_xMg_{1-x}PO_4$ (Sample 5)		51	

Journal Pre-proof

CIE L*a*b* colorimetry of powder pigments

Table 4 illustrates the colorimetric parameters of the samples for color evaluation. The sample with the lightest hue was magnesium phosphate (Sample 1), exhibiting the lowest color saturation (C*). The insertion of cobalt into the structure of Sample 1 modified both the chromatic parameters (a* and b*) and the color saturation. The total color variation (ΔE) in Sample 2 was 9.87, considered a substantial difference and quite perceptible to the human eye ($6 \leq \Delta E < 12$).[26] Sample 5 showed the highest color saturation and lowest luminosity, along with the most significant color difference relative to Sample 1, suggesting that the color is more saturated when Na+ and Li+ are present in the pigment, due to a structure that favors d-d electronic transitions of Co^{2+} ions.

In terms of reproducibility, the synthesis has already been performed more than once, and the colorimetric data have been analyzed. In two times of analysis for the samples, the total color difference (ΔE*ab) obtained a "very clear" color difference intensity (ΔE=3.0-6.0), according to Horsth et al 2021[26].

Table 4. Colorimetric parameters of powdered pigments and the photographic illustration

Samples	Colorimetric Parameters					Color by software	Pigments
	L*	a*	b*	C*	ΔE		
Sample 1	*75.35*	*-0.19*	*0.13*	0.23	-	⬜	
Sample 2	*76.41*	*4.23*	*-8.63*	9.61	9.87	🟪	
Sample 3	*69.04*	*16.87*	*-18.75*	25.22	26.22	🟪	
Sample 4	*70.97*	*17.43*	*-18.35*	25.51	25.91	🟪	
Sample 5	*14.25*	*13.64*	*-79.58*	80.74	101.38	🟦	

Figure 11 shows that the synthesized pigments have their colorimetric parameters in the red/blue color quadrant (+a*/-b*) within the CIEL*a*b* color space, resulting in the observed purple color. The color tone is mainly influenced by the amount of cobalt and its interaction with other dopant ions.[81]

The respective pigments have been proposed as cold pigments for solar NIR reflectance, effective in regions of high solar radiation. The paint used for this purpose is made up of five chemical inputs: polymers, plasticizers, additives, pigments and solvents. Water is used as a solvent and accounts for the largest percentage in the composition of these cold paints (around 80%). Pigments are added to improve the reflective performance of the paints, and can be as little as 10% of the paint's composition[82,83]. Colorimetry of pigments was also repeated after heating at 1000 °C and the total color difference (ΔE*ab) of the pigments after the calcination process was calculated. Obtaining an intensity of the color difference "clear" (ΔE=3.0)[26].

Journal Pre-proof

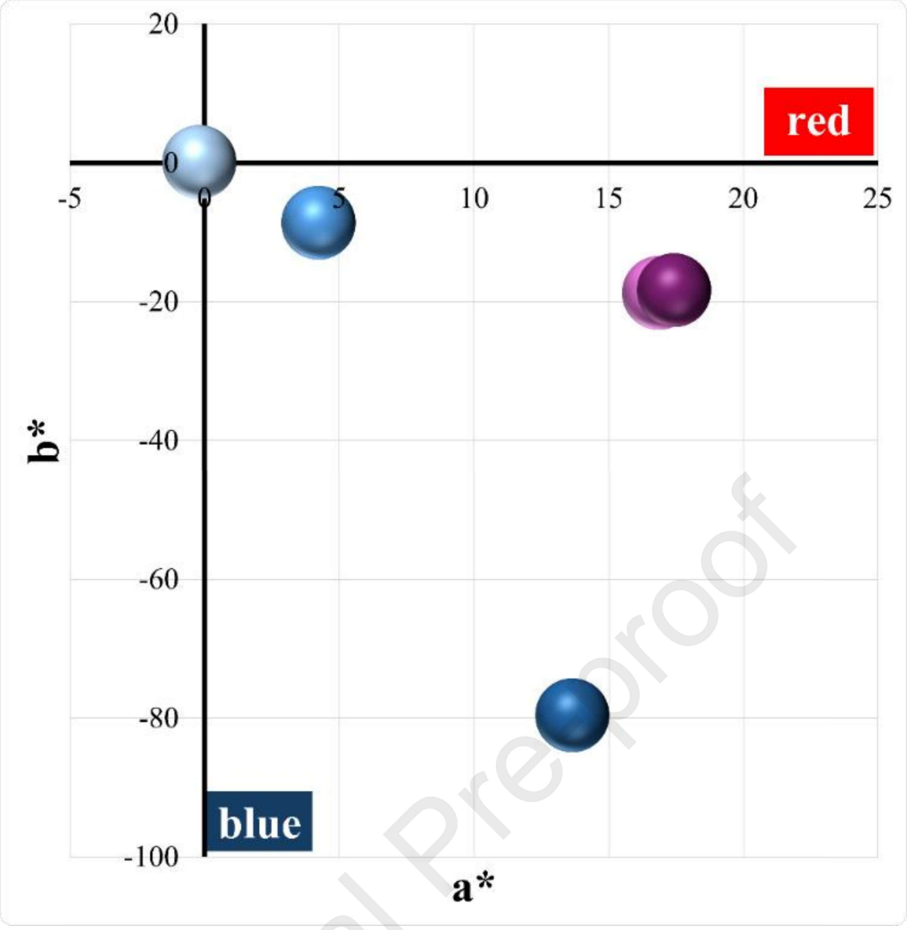

Figure 11. Graph of colorimetric parameters red (+a) versus blue (-b).

Journal Pre-proof

Conclusion

In summary, grey (Sample 1 and Sample 2), pink (Sample 3 and Sample 4), and purple (Sample 5) pigments were successfully synthesized. Cassava starch was used as a sustainable alternative to synthetic gelling agents during combustion, creating uniformly colored metallophosphate pigments. Combining phosphates with alkaline dopants enhanced the pigment saturation while maintaining a consistent concentration of the chromophore ion (Co).

Moreover, the synthesized material exhibited promising optical characteristics, with three samples showing reflectance exceeding 60%, making them suitable for use as pigments in thermal coatings. The importance of post-calcination pigment cleaning to optimize their chromatic properties was also demonstrated. The thermal stability tests showed that the pigments retained the same phases after high-temperature calcination and exhibited a low total color variation, indicating excellent quality. The findings highlight the promising potential of cassava starch-based metallophosphate pigments with enhanced NIR reflectance for applications in reflective coatings, offering a sustainable and effective solution for passive cooling in building interiors.

Acknowledgments

Balaba appreciates Capes for a graduate scholarship. Anaissi is thankful for a CNPq Productivity grant (310815/2022-3) and the CNPq grant (427127/2018-1). Anaissi and Bittencourt are grateful for a WBI/Confap-Fundação Araucária (BEL2023081000001).

Contributor Roles

Conceptualization: N. Balaba, J. O. Primo, D. F. L. Horsth, F. J. Anaissi; Data curation: N. Balaba, J. O. Primo, D. F. L. Horsth; Formal analysis: N. Balaba, J. O. Primo, D. F. L. Horsth, P. Umek; Funding acquisition: C. Bittencourt, F. J. Anaissi; Investigation: N. Balaba, J. O. Primo, D. F. L. Horsth; Methodology: N. Balaba, J. O. Primo; Project administration: C. Bittencourt, F. J. Anaissi; Resources and Supervision: C. Bittencourt, F. J. Anaissi; Visualization Writing – original draft: N. Balaba, J. O. Primo, D. F. L. Horsth, P. Umek, C. Bittencourt; Writing – review & editing: N. Balaba, J. Anaissi

Journal Pre-proof

References

[1] M.J. Deepa, S.R. Arunima, L. Elias, T.C. Bhagya, C. V. Geethanjali, V.S. Saji, S.M. Aboobakar Shibli, BiVO4-TiO2Composite-Based Zinc Phosphate Coating for High NIR Reflectance and Sustainable Energy-Saving Applications, Ind. Eng. Chem. Res. (2022). https://doi.org/10.1021/ACS.IECR.2C00504/ASSET/IMAGES/LARGE/IE2C00504_0013.JPEG.

[2] S. Rossi, M. Calovi, D. Dalpiaz, M. Fedel, The Influence of NIR Pigments on Coil Coatings' Thermal Behaviors, Coatings 2020, Vol. 10, Page 514 10 (2020) 514. https://doi.org/10.3390/COATINGS10060514.

[3] P.K. Thejus, K. V. Krishnapriya, K.G. Nishanth, NIR reflective, anticorrosive magenta pigment for energy saving sustainable building coatings, Solar Energy 222 (2021) 103–114. https://doi.org/10.1016/J.SOLENER.2021.05.017.

[4] M. Zang, L. Feng, Z. Zeng, Y. Yang, X. Sun, Environmentally Friendly High-Near-Infrared Reflectance Blue Pigment YIn0.9- xMn0.1MxO3-δBased on Li/Zn Doping, ACS Sustain. Chem. Eng. 10 (2022) 13877–13886. https://doi.org/10.1021/ACSSUSCHEMENG.2C04967/ASSET/IMAGES/LARGE/SC2C04967_0010.JPEG.

[5] J. de O. Primo, K.W. Borth, D.C. Peron, V. de C. Teixeira, D. Galante, C. Bittencourt, F.J. Anaissi, Synthesis of green cool pigments (CoxZn1-xO) for application in NIR radiation reflectance, J. Alloys Compd. 780 (2019) 17–24. https://doi.org/10.1016/j.jallcom.2018.11.358.

[6] C. Ding, A. Han, M. Ye, Y. Zhang, L. Yao, J. Yang, Hydrothermal synthesis and characterization of novel yellow pigments based on V5+ doped BiPO4 with high near-

infrared reflectance, RSC Adv. 8 (2018) 19690–19700. https://doi.org/10.1039/C8RA02406E.

[7] P.K. Thejus, B. Koley, K.G. Nishanth, An intense purple chromophore based on Co2+ in distorted tetrahedral coordination, Dyes and Pigments 158 (2018) 267–276. https://doi.org/10.1016/J.DYEPIG.2018.05.054.

[8] D.F.L. Horsth, J. de O. Primo, N. Balaba, F.J. Anaissi, C. Bittencourt, Color stability of blue aluminates obtained from recycling and applied as pigments, RSC Sustainability 1 (2023) 159–166. https://doi.org/10.1039/d2su00057a.

[9] M.Á. Tena, R. Mendoza, C. Trobajo, S. García-Granda, Cobalt Minimisation in Violet Co3P2O8 Pigment, Materials 15 (2022) 1111. https://doi.org/10.3390/ma15031111.

[10] P.K. Thejus, B. Koley, K.G. Nishanth, An intense purple chromophore based on Co2+ in distorted tetrahedral coordination, Dyes and Pigments 158 (2018) 267–276. https://doi.org/10.1016/J.DYEPIG.2018.05.054.

[11] A. Piçarra, I.R. Annesley, A. Otsuki, R. de Waard, Market assessment of cobalt: Identification and evaluation of supply risk patterns, Resources Policy 73 (2021) 102206. https://doi.org/10.1016/J.RESOURPOL.2021.102206.

[12] E. Shoko, Y. Dang, G. Han, B.B. Duff, M.S. Dyer, L.M. Daniels, R. Chen, F. Blanc, J.B. Claridge, M.J. Rosseinsky, Polymorph of $LiAlP_2O_7$: Combined Computational, Synthetic, Crystallographic, and Ionic Conductivity Study, Inorg. Chem. 60 (2021) 14083–14095. https://doi.org/10.1021/acs.inorgchem.1c01396.

[13] A. López-Grande, G.C. Mather, F. Muñoz, Thermodynamic calculation of the ionic conductivity of LiPON glasses and solid electrolytes, J. Mater. Chem. A Mater. 11 (2023) 12282–12296. https://doi.org/10.1039/D3TA00724C.

[14] M. Ma, M. Du, Y. Liu, H. Lü, J. Yang, Z. Hao, J. Guo, X. Wu, Electrode particulate materials for advanced rechargeable batteries: A review, Particuology 86 (2024) 160–181. https://doi.org/10.1016/j.partic.2023.05.006.

[15] V. Elakkiya, S. Sumathi, Bismuth and Vanadium-Substituted Yttrium Phosphates for Cool Coating Applications, ACS Omega 7 (2022) 44266–44277. https://doi.org/10.1021/ACSOMEGA.2C05748/ASSET/IMAGES/LARGE/AO2C05748_0016.JPEG.

[16] Henrique Eisi Toma, Química de coordenação, organometálica e catálise, 1st ed., Blusher, São Paulo, 2013.

[17] K. Fang, J. Zhu, Q. Xie, Y. Men, W. Yang, J. Li, X. Yu, Synthesis of Fe2+ Substituted High-Performance LiMn1−xFexPO4/C (x = 0, 0.1, 0.2, 0.3, 0.4) Cathode Materials for Lithium-Ion Batteries via Sol-Gel Processes, Molecules 26 (2021) 7641. https://doi.org/10.3390/molecules26247641.

[18] Z. Li, H. Sun, W. Wei, F. Liu, X. Xu, Z. Liu, Synthesis of ultrathin carbon layer-coated LiNiPO4 nanoparticles by solvothermal method, Ceram. Int. 50 (2024) 24995–25004. https://doi.org/10.1016/j.ceramint.2024.04.186.

[19] N.D. Zhigadlo, Exploring 2D materials by high pressure synthesis: hBN, Mg-hBN, b-P, b-AsP, and GeAs, J. Cryst. Growth 631 (2024). https://doi.org/10.1016/j.jcrysgro.2024.127627.

[20] R. Naik, A. Naveen Kumar, Y. V. Naik, N. Basavaraju, G. V. Ashok Reddy, H.P. Nagaswarupa, B. Ali Al-Asbahi, N. Roy, S. Woo Joo, Green combustion synthesis of multifunctional inorganic ZnO: Co2+ (1–11 mol%) nanoparticles: Electrochemical and photocatalytic applications, Inorganica Chim. Acta 563 (2024). https://doi.org/10.1016/j.ica.2024.121924.

[21] L. Guo, R. Lei, T.C. Zhang, D. Du, W. Zhan, Insight into the role and mechanism of polysaccharide in polymorphous magnesium oxide nanoparticle synthesis for arsenate

Journal Pre-proof

removal, Chemosphere 296 (2022) 133878. https://doi.org/10.1016/J.CHEMOSPHERE.2022.133878.

[22] A.F. Chamorro, M. Palencia, T.A. Lerma, Physicochemical Characterization and Properties of Cassava Starch: A Review, Polymers (Basel). 17 (2025) 1663. https://doi.org/10.3390/polym17121663.

[23] M. Zhang, L. Feng, Z. Zeng, Y. Yang, X. Sun, Environmentally Friendly High-Near-Infrared Reflectance Blue Pigment $YIn_{0.9-x}Mn_{0.1}M_xO_{3-\delta}$ Based on Li/Zn Doping, ACS Sustain. Chem. Eng. 10 (2022) 13877–13886. https://doi.org/10.1021/acssuschemeng.2c04967.

[24] Y. Xiao, L. Feng, B. Huang, J. Chen, W. Xie, X. Sun, Synthesis and characterization of multi-colored pigments of LiRE(MoO4+δ)2 (RE = Ce, Pr, Nd, Er) with high near-infrared reflectance, Ceram. Int. 47 (2021) 29856–29863. https://doi.org/10.1016/j.ceramint.2021.07.158.

[25] C.A. Gueymard, Revised composite extraterrestrial spectrum based on recent solar irradiance observations, Solar Energy 169 (2018) 434–440. https://doi.org/10.1016/j.solener.2018.04.067.

[26] D.F.L. Horsth, J.O. Primo, M. Dalpasquale, C. Bittencourt, F.J. Anaissi, Colored aluminates pigments obtained from metallic aluminum waste, an opportunity in the circular economy, Clean. Eng. Technol. 5 (2021) 100313. https://doi.org/10.1016/J.CLET.2021.100313.

[27] G. Sharma, W. Wu, E.N. Dalal, The CIEDE2000 color-difference formula: Implementation notes, supplementary test data, and mathematical observations, Color Res. Appl. 30 (2005) 21–30. https://doi.org/10.1002/col.20070.

[28] M. Quindici, O segredodas cores, All Print, São Paulo, 2013.

[29] D.F.L. Horsth, J. de O. Primo, J.S. Correa, F.J. Anaissi, X. Noirfalise, C. Bittencourt, Upcycling can seals into high-value boehmite-like for the synthesis of MnAl2O4: A circular economy approach, Next Sustainability 2 (2023) 100009. https://doi.org/10.1016/j.nxsust.2023.100009.

[30] M. Muhammad, R. Ma, A. Du, Y. Fan, X. Zhao, N. Jun, X. Cao, Effect of Temperature on the Morphology and Corrosion Resistance of Modified Boron Nitride Nanosheets Incorporated into Steel Phosphate Coating, Metals (Basel). 13 (2023). https://doi.org/10.3390/met13071186.

[31] P. Zhang, S. Xu, Y. Wang, W. Zhang, W. Li, C. Wei, P. Zhang, S. Miao, Fabrication of Pd/Mg2P2O7 via a Struvite-Template Way from Wastewater and Application as Chemoselective Catalyst in Hydrogenation of Nitroarenes, Chemistry – A European Journal 27 (2021) 10666–10676. https://doi.org/10.1002/CHEM.202100684.

[32] R. Mahajan, R. Prakash, A review report on structural and optical characterization of rare earth/transition metal doped pyrophosphate phosphors, Journal of Materials Science: Materials in Electronics 33 (2022) 25491–25517. https://doi.org/10.1007/S10854-022-09279-2/FIGURES/11.

[33] A. Ananda, T. Ramakrishnappa, S. Archana, L.S.R. Yadav, B.M. Shilpa, G. Nagaraju, B.K. Jayanna, Materials Today : Proceedings Green synthesis of MgO nanoparticles using Phyllanthus emblica for Evans blue degradation and antibacterial activity, Mater. Today Proc. (2021). https://doi.org/10.1016/j.matpr.2021.05.340.

[34] W. Zhou, L. Xue, X. Lü, H. Gao, Y. Li, S. Xin, G. Fu, Z. Cui, Y. Zhu, J.B. Goodenough, NaxMV(PO4)3 (M = Mn, Fe, Ni) Structure and Properties for Sodium Extraction, Nano Lett. 16 (2016) 7836–7841. https://doi.org/10.1021/ACS.NANOLETT.6B04044/SUPPL_FILE/NL6B04044_SI_004.CIF.

Journal Pre-proof

[35] Keskin, M. Türemiş, M. Katı, S. Gültekin, Y. Tuncer Arslanlar, A. Çetin, R. Kibar, Detailed luminescence (RL, PL, CL, TL) behaviors of Tb3+ and Dy3+ doped LiMgPO4 synthesized by sol-gel method, J. Lumin. 225 (2020) 117276. https://doi.org/10.1016/J.JLUMIN.2020.117276.

[36] C. Neef, H.P. Meyer, R. Klingeler, Morphology-controlled two-step synthesis and electrochemical studies on hierarchically structured LiCoPO4, Solid State Sci. 48 (2015) 270–277. https://doi.org/10.1016/J.SOLIDSTATESCIENCES.2015.08.021.

[37] K.O. Kongshaug, H. Fjellv#, K.P. Lillerud, The synthesis and crystal structure of two novel 3D open-framework zinc phosphates UiO-21 and UiO-22, n.d. www.elsevier.nl/locate/micromeso.

[38] M. Llusar, A. Zielinska, M.A. Tena, J.A. Badenes, G. Monrós, Blue-violet ceramic pigments based on Co and Mg Co2−xMgxP2O7 diphosphates, J. Eur. Ceram. Soc. 30 (2010) 1887–1896. https://doi.org/10.1016/J.JEURCERAMSOC.2010.03.017.

[39] L. Lin, T. Wanjun, Effects of Tb3+ doping on luminescence properties of NaMg4(PO4)3:Eu2+, J. Lumin. 198 (2018) 405–409. https://doi.org/10.1016/J.JLUMIN.2018.03.001.

[40] S.C. Kim, M.S. Lee, J. Kang, Y. Il Kim, S.J. Kim, Crystal structure and ion conductivity of a new mixed-anion phosphate LiMg3(PO4)P2O7, J. Solid State Chem. 225 (2015) 335–339. https://doi.org/10.1016/J.JSSC.2015.01.011.

[41] M.K. Devaraju, Q.D. Truong, H. Hyodo, T. Tomai, I. Honma, Supercritical Fluid Synthesis of LiCoPO4 Nanoparticles and Their Application to Lithium Ion Battery, Inorganics 2014, Vol. 2, Pages 233-247 2 (2014) 233–247. https://doi.org/10.3390/INORGANICS2020233.

[42] W. Gieszczyk, B. Marczewska, M. Kłosowski, A. Mrozik, P. Bilski, A. Sas-Bieniarz, P. Goj, P. Stoch, Thermoluminescence Enhancement of LiMgPO4 Crystal Host by Tb3+ and Tm3+ Trivalent Rare-Earth Ions Co-doping, Materials 2019, Vol. 12, Page 2861 12 (2019) 2861. https://doi.org/10.3390/MA12182861.

[43] J. Ludwig, C. Alarcón-Suesca, S. Geprägs, D. Nordlund, M.M. Doeff, I.P. Orench, T. Nilges, Direct synthesis and characterization of mixed-valent Li0.5−δCoPO4, a Li-deficient derivative of the Cmcm polymorph of LiCoPO4, RSC Adv. 7 (2017) 28069–28081. https://doi.org/10.1039/C7RA04043A.

[44] S. Meseguer, M.A. Tena, C. Gargori, J.A. Badenes, M. Llusar, G. Monrós, Structure and colour of cobalt ceramic pigments from phosphates, Ceram. Int. 33 (2007) 843–849. https://doi.org/10.1016/j.ceramint.2006.01.024.

[45] N. Gorodylova, Ž. Dohnalová, P. Šulcová, P. Bělina, M. Vlček, Influence of synthesis conditions on physicochemical parameters and corrosion inhibiting activity of strontium pyrophosphates SrMIIP2O7 (MII = Mg and Zn), Prog. Org. Coat. 93 (2016) 77–86. https://doi.org/10.1016/j.porgcoat.2016.01.004.

[46] K. Przywecka, B. Grzmil, K. Kowalczyk, J. Sreńscek-Nazzal, Studies on preparation of phosphate pigments for application in composite protective coatings, Prog. Org. Coat. 119 (2018) 44–49. https://doi.org/10.1016/j.porgcoat.2018.02.009.

[47] Y. Zhao, J. Zhang, Microstrain and grain-size analysis from diffraction peak width and graphical derivation of high-pressure thermomechanics, J. Appl. Crystallogr. 41 (2008) 1095–1108. https://doi.org/10.1107/S0021889808031762.

[48] M. Hoffmann, M. Zier, S. Oswald, J. Eckert, Challenges for lithium species identification in complementary Auger and X-ray photoelectron spectroscopy, J. Power Sources 288 (2015) 434–440. https://doi.org/10.1016/j.jpowsour.2015.04.144.

[49] L.H. Grey, H.-Y. Nie, M.C. Biesinger, Defining the nature of adventitious carbon and improving its merit as a charge correction reference for XPS, Appl. Surf. Sci. 653 (2024) 159319. https://doi.org/10.1016/j.apsusc.2024.159319.

Journal Pre-proof

[50] G.A. Castillo Rodriguez, K.S. Zambrano, M. Hernández, J. Aguilar Martinez, C. Gómez Rodríguez, XPS Study Calcining Mixtures of Brucite with Titania, n.d.

[51] F.J. García-Mateos, R. Berenguer, M.J. Valero-Romero, J. Rodríguez-Mirasol, T. Cordero, Phosphorus functionalization for the rapid preparation of highly nanoporous submicron-diameter carbon fibers by electrospinning of lignin solutions, J. Mater. Chem. A Mater. 6 (2018) 1219–1233. https://doi.org/10.1039/c7ta08788h.

[52] Y. Yao, B. Gao, J. Chen, L. Yang, Engineered biochar reclaiming phosphate from aqueous solutions: Mechanisms and potential application as a slow-release fertilizer, Environ. Sci. Technol. 47 (2013) 8700–8708. https://doi.org/10.1021/es4012977.

[53] K. Li, W. Dong, Q. Liu, G. Lv, M. Xie, X. Sun, L. Qiu, J. Lin, A biotin receptor-targeted silicon(IV) phthalocyanine for in vivo tumor imaging and photodynamic therapy, J. Photochem. Photobiol. B 190 (2019) 1–7.

[54] X. Wu, K. Gong, G. Zhao, W. Lou, X. Wang, W. Liu, Mechanical synthesis of chemically bonded phosphorus-graphene hybrid as high-temperature lubricating oil additive, RSC Adv. 8 (2018) 4595–4603. https://doi.org/10.1039/c7ra11691h.

[55] C. Koventhan, V. Vinothkumar, S.-M. Chen, P. Veerakumar, K.-C. Lin, Polyol-assisted synthesis of spinel-type magnesium cobalt oxide nanochains for voltammetric determination of the antipsychotic drug thioridazine, Journal of Electroanalytical Chemistry 898 (2021) 115600. https://doi.org/10.1016/j.jelechem.2021.115600.

[56] Y.C. Lu, E.J. Crumlin, G.M. Veith, J.R. Harding, E. Mutoro, L. Baggetto, N.J. Dudney, Z. Liu, Y. Shao-Horn, In situ ambient pressure X-ray photoelectron spectroscopy studies of lithium-oxygen redox reactions, Sci. Rep. 2 (2012). https://doi.org/10.1038/srep00715.

[57] S. Oswald, F. Thoss, M. Zier, M. Hoffmann, T. Jaumann, M. Herklotz, K. Nikolowski, F. Scheiba, M. Kohl, L. Giebeler, D. Mikhailova, H. Ehrenberg, Binding energy referencing for XPS in Alkali metal-based battery materials research (II): Application to complex composite electrodes, Batteries 4 (2018). https://doi.org/10.3390/batteries4030036.

[58] D. Cabrera-German, G. Gomez-Sosa, A. Herrera-Gomez, Accurate peak fitting and subsequent quantitative composition analysis of the spectrum of Co 2p obtained with Al Kα radiation: I: cobalt spinel, Surface and Interface Analysis 48 (2016) 252–256. https://doi.org/10.1002/sia.5933.

[59] J.X. Flores-Lasluisa, J. Quílez-Bermejo, A.C. Ramírez-Pérez, F. Huerta, D. Cazorla-Amorós, E. Morallón, Copper-doped cobalt spinel electrocatalysts supported on activated carbon for hydrogen evolution reaction, Materials 12 (2019). https://doi.org/10.3390/ma12081302.

[60] J. Ludwig, C. Alarcón-Suesca, S. Geprägs, D. Nordlund, M.M. Doeff, I.P. Orench, T. Nilges, Direct synthesis and characterization of mixed-valent Li 0.5−δ CoPO 4 , a Li-deficient derivative of the Cmcm polymorph of LiCoPO 4, RSC Adv. 7 (2017) 28069–28081. https://doi.org/10.1039/C7RA04043A.

[61] H. Mao, F. Zhang, X. Liu, J. Qiu, B. Li, Z. Jin, Synthesis of cobalt phosphate nanoflakes for high-performance flexible symmetric supercapacitors, Journal of Materials Science: Materials in Electronics 29 (2018) 16721–16729. https://doi.org/10.1007/s10854-018-9765-x.

[62] H.T.T. Nguyen, D. Jung, C.-Y. Park, D.J. Kang, Synthesis of single-crystalline sodium vanadate nanowires based on chemical solution deposition method, Mater. Chem. Phys. 165 (2015) 19–24. https://doi.org/10.1016/j.matchemphys.2015.05.053.

[63] K. Sotiriadis, P. Mácová, A.S. Mazur, P.M. Tolstoy, A. Viani, A solid state NMR and in-situ infrared spectroscopy study on the setting reaction of magnesium sodium phosphate

Journal Pre-proof

cement, J. Non. Cryst. Solids 498 (2018) 49–59. https://doi.org/10.1016/j.jnoncrysol.2018.06.006.

[64] I. Konidakis, C.P.E. Varsamis, E.I. Kamitsos, D. Möncke, D. Ehrt, Structure and properties of mixed strontium-manganese metaphosphate glasses, Journal of Physical Chemistry C 114 (2010) 9125–9138. https://doi.org/10.1021/jp101750t.

[65] A.M. Abdelghany, F.H. Elbatal, H.A. Elbatal, F.M. EzzElDin, Optical and FTIR structural studies of CoO-doped sodium borate, sodium silicate and sodium phosphate glasses and effects of gamma irradiation - A comparative study, J. Mol. Struct. 1074 (2014) 503–510. https://doi.org/10.1016/j.molstruc.2014.06.011.

[66] J. Mcmurry, QUÍMICA ORGÁNICA, 2008.

[67] M. Malakauskaite-Petruleviciene, Z. Stankeviciute, G. Niaura, E. Garskaite, A. Beganskiene, A. Kareiva, Characterization of sol-gel processing of calcium phosphate thin films on silicon substrate by FTIR spectroscopy, Vib. Spectrosc. 85 (2016) 16–21. https://doi.org/10.1016/j.vibspec.2016.03.023.

[68] R.K. Brow, Section 1. Structure Review: the structure of simple phosphate glasses, n.d. www.elsevier.com/locate/jnoncrysol.

[69] S. Türk, I. Altınsoy, G.Ç. Efe, M. Ipek, M. Özacar, C. Bindal, Biomimetic synthesis of Ag, Zn or Co doped HA and coating of Ag, Zn or Co doped HA/fMWCNT composite on functionalized Ti, Materials Science and Engineering C 99 (2019) 986–998. https://doi.org/10.1016/j.msec.2019.02.025.

[70] B.C. Cornilsen, R.A. Condrate, The vibrational spectra of magnesium pyrophosphate polymorphs, Journal of Physics and Chemistry of Solids 38 (1977) 1327–1332. https://doi.org/10.1016/0022-3697(77)90003-8.

[71] H. Begam, S. Dasgupta, S. Bodhak, A. Barui, Cobalt doped biphasic calcium phosphate ceramics for bone regeneration applications: Assessment of in vitro antibacterial activity, biocompatibility, osteogenic and angiogenic properties, Ceram. Int. 50 (2024) 13276–13285. https://doi.org/10.1016/j.ceramint.2024.01.240.

[72] A. Masegosa, M.A. Palacios, E. Ruiz, S. Gómez-Coca, J. Krzystek, J.M. Moreno, E. Colacio, Dinuclear CoIIYIIIvs. tetranuclear CoII2YIII2 complexes: the effect of increasing molecular size on magnetic anisotropy and relaxation dynamics, Dalton Transactions 48 (2019) 14873–14884. https://doi.org/10.1039/C9DT02969A.

[73] M. Ardit, G. Cruciani, M. Dondi, Structural relaxation in tetrahedrally coordinated Co2+ along the gahnite-Co-aluminate spinel solid solution, American Mineralogist 97 (2012) 1394–1401. https://doi.org/10.2138/AM.2012.4093.

[74] J. de O. Primo, D.F.L. Horsth, N. Balaba, P. Umek, F.J. Anaissi, C. Bittencourt, Synthesis of Blue Gahnite (ZnAl2O4:Co, Nd): A Cost-Effective Method for Producing Solar-Reflective Pigments for Cool Coatings, Materials 16 (2023) 1696. https://doi.org/10.3390/MA16041696/S1.

[75] L. De Bruecker, prof Veronique Van Speybroeck, Influence of the number of ligands and point group on the electronic structure of Co 2+ aqua-complexes, 2022. https://doi.org/https://doi.org/10.1021/acs.inorgchem.2c02358.

[76] V. Elakkiya, S. Sumathi, Vanadium and bismuth doped FePO4 as Near Infra Red (NIR) reflective pigment for energy saving application, Mater. Chem. Phys. 290 (2022) 126561. https://doi.org/10.1016/j.matchemphys.2022.126561.

[77] R. Ianoş, E. Muntean, C. Păcurariu, R. Lazău, C. Bandas, G. Delinescu, Combustion synthesis of a blue Co-doped zinc aluminate near-infrared reflective pigment, Dyes and Pigments 142 (2017) 24–31. https://doi.org/10.1016/j.dyepig.2017.03.016.

[78] P.K. Thejus, K. V. Krishnapriya, K.G. Nishanth, NIR reflective, anticorrosive magenta pigment for energy saving sustainable building coatings, Solar Energy 222 (2021) 103–114. https://doi.org/10.1016/J.SOLENER.2021.05.017.

Journal Pre-proof

[79] P.K. Thejus, B. Koley, K.G. Nishanth, An intense purple chromophore based on Co2+ in distorted tetrahedral coordination, Dyes and Pigments 158 (2018) 267–276. https://doi.org/10.1016/J.DYEPIG.2018.05.054.

[80] J. Yun, K.Y. Jung, Near-infrared reflective Mg0.5Co0.5-xMnxAl2O4 black pigment synthesized by spray pyrolysis: Optimization of composition and calcination temperature, Ceram. Int. 50 (2024) 25013–25024. https://doi.org/10.1016/j.ceramint.2024.04.226.

[81] H. Lakhlifi, Y. El Jabbar, R. El Ouatib, L. Er-Rakho, S. Guillemet-Fritsch, B. Durand, Structural, morphological and optical properties of cobalt-substituted MgMoO4 ceramics prepared by pyrolysis of citric acid precursors, Surfaces and Interfaces 21 (2020) 100718. https://doi.org/10.1016/J.SURFIN.2020.100718.

[82] E. Shittu, V. Stojceska, P. Gratton, M. Kolokotroni, Environmental impact of cool roof paint: case-study of house retrofit in two hot islands, Energy Build. 217 (2020) 7. https://doi.org/10.1016/j.enbuild.2020.110.

[83] M. Santamouris, Cooling the cities - A review of reflective and green roof mitigation technologies to fight heat island and improve comfort in urban environments, Solar Energy 103 (2014) 682–703. https://doi.org/10.1016/j.solener.2012.07.003.

Journal Pre-proof

Highlights

- Eco-friendly cobalt phosphate pigments were prepared via starch-assisted synthesis.
- Phosphate pigments showed promising cool coating optical performance.
- NIR reflectance reached 75% for $Co_xMg_{1-x}PO_4$ compositions.
- Cassava starch favored particle dispersion and surface homogeneity.
- The synthesized pigments are promising for energy-saving coating applications.

Journal Pre-proof

Declaration of interests

☐ The authors declare that they have no known competing financial interests or personal relationships that could have appeared to influence the work reported in this paper.

☒ The authors declare the following financial interests/personal relationships which may be considered as potential competing interests:

Fauze Jaco Anaissi reports financial support was provided by State University of the Central-West. If there are other authors, they declare that they have no known competing financial interests or personal relationships that could have appeared to influence the work reported in this paper.

Journal Pre-proof